On the origin of Si nanocrystal formation in a Si suboxide matrix

Decai Yu, Sangheon Lee, and Gyeong S. Hwang[a)]
Department of Chemical Engineering, The University of Texas, Austin, Texas 78712, USA

(Received 19 December 2007; accepted 4 September 2007; published online 26 October 2007)

We examined mechanisms underlying Si nanocrystal formation in Si-rich SiO_2 using a combination of quantum mechanical and Monte Carlo (MC) simulations. We find that this process is mainly driven by suboxide penalty arising from incomplete O coordination, with a minor contribution of strain, and it is primarily controlled by O diffusion rather than excess Si diffusion and agglomeration. The overall behavior of Si cluster growth from our MC simulations based on these fundamental findings agrees well with experiments. © *2007 American Institute of Physics*. [DOI: 10.1063/1.2800268]

I. INTRODUCTION

The discovery of efficient room temperature luminescence from silicon nanocrystals (nc-Si) embedded in an amorphous silicon oxide (a-SiO_x) matrix[1,2] has generated significant interest in the nc-Si/a-SiO_x system because of its potential applications in electronic, optoelectronic, and optical devices in Si-compatible technology.[3–7] Earlier experimental investigations suggested that the absorption and luminescence properties of oxide embedded Si nanocrystals are governed by a complex combination of the size, shape, and size distribution of Si nanocrystals; the atomic structure, bonding, and defects at the crystal-matrix interface; and the composition and structure of the oxide matrix.[8] This implies that atomic-level control of such structural properties will offer great opportunities in development of nc-Si based devices. At present, however, many fundamental aspects of the synthesis and structure of nc-Si embedded in a-SiO_x are still uncertain, despite significant efforts over recent years.

High temperature annealing of amorphous Si-rich SiO_2 (a-SiO_x, $x<2$) has been widely used to synthesize embedded Si nanocrystals.[9–12] The formation of nanocrystals has often been described by the nucleation, growth, and Ostwald ripening of Si precipitates in the oxide matrix.[12,13] However, this model fails to explain some important characteristics in nc-Si growth, including strong nc-Si size dependence on initial Si supersaturation and rapid nc-Si formation at the early stage of annealing with very slow ripening.[12] Note that, according to the Ostwald ripening theory, the nc-Si size is primarily determined by the thermal stability difference between different sizes of nanocrystals rather than the amount of excess Si atoms. In addition, the major driving force of nc-Si formation has not been clarified.

In this paper, we attempt to identify mechanisms underlying Si nanocluster formation in a Si suboxide matrix during high temperature thermal treatment. We first present the driving force of Si cluster formation, particularly the effect of strain and suboxide penalty as well as the role of diffusion of O and Si atoms. Then, based on the fundamental findings, we present a kinetic model for the formation of Si clusters in a-SiO_x, with a qualitative comparison between our simulation results and experimental observations available in the literature.

II. MAJOR DRIVING FORCE

Recent theoretical studies[14] have predicted that excess Si atoms in a-SiO_2 are incorporated into the Si–O bond network, rather than undergo diffusion and agglomeration. This suggests that Si cluster formation in a-SiO_x is attributed primarily to chemical phase separation into Si and SiO_2. Thus, to determine the major driving force of the phase separation we calculated changes in the total energy of suboxide matrix with varying Si/O ratios.

We used the continuous random network (CRN) model[15] to construct defect-free model structures of a-SiO_x. Each periodic supercell consists of 64 Si atoms and corresponding O atoms at a given Si/O ratio, with a volume (V) given by

$$V = V_{Si}(N_{Si} - N_O/2) + V_{SiO_2} \times N_O/2,$$

where N_{Si} and N_O are the number of Si and O atoms, respectively. The unit volumes of a-Si (V_{Si}) and a-SiO_2 (V_{SiO_2}) are extracted, respectively, from corresponding experimental densities of 2.28 g/cm^3 (Ref. 16) and 2.2 g/cm^3.[17] Starting with a randomized configuration, each suboxide system was relaxed via a sequence of bond switching based on metropolis Monte Carlo (MMC) sampling. Using Keating-like potentials,[18] bond transpositions were performed at temperatures of 5000, 3000, and 1000 K sequentially with approximately 850N, 600N, and 200N trials, respectively, where N is the total number of Si and O atoms in the supercell. Overall, calculated structural factors from this approach agree well with previous experimental measurements and other simulation results available in the literature. For instance, our calculations yielded an average Si–Si–Si bond angle of $\approx 109.3°$ with a standard deviation of $\approx 10°$ in a-Si, and an average Si–O–Si bond angle of $\approx 150°$ with a standard deviation of $\approx 11°$ in a-SiO_2, in good agreement with experiments.[16,17]

We also used density functional calculations to further relax the CRN structures. All structures and energetics reported herein were calculated using Vienna *ab initio* simulation package (VASP),[19] a planewave density functional

[a)]Author to whom correspondence should be addressed. Electronic mail: gshwang@che.utexas.edu

 © 2007 American Institute of Physics

Downloaded 02 Sep 2010 to 146.6.194.60. Redistribution subject to AIP license or copyright; see http://jap.aip.org/about/rights_and_permissions

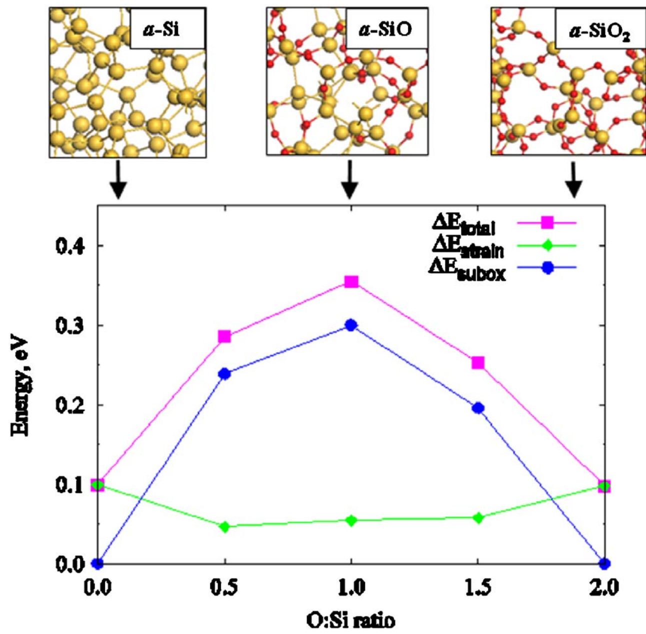

FIG. 1. (Color online) Variation in the relative energies of SiO_x ($0 \leqslant x \leqslant 2$) with respect to *c*-Si and *c*-SiO_2 (β-crystobalite) energies as a function of the O:Si ratio. For each suboxide system, the total increase in the relative energy (ΔE_{tot}) is obtained by subtracting the Si–Si (in *c*-Si) and Si–O (in β-crystobalite) bond energies from the total energy. The suboxide energy (ΔE_{subox}) represents the sum of suboxide penalty energies of Si atoms in +1, +2, +3 oxidation states and the strain energy (ΔE_{strain}) is the difference between ΔE_{tot} and ΔE_{subox}. In this analysis, for 64 Si atoms per supercell, the numbers of Si^0, Si^+, Si^{2+}, Si^{3+}, and Si^{4+} are (64, 0, 0, 0, 0), (13, 39, 11, 1, 0), (0, 18, 29, 16, 1), (0, 2, 11, 36, 15), and (0, 0, 0, 0, 64) for O/Si ratios of 0, 0.5, 1, 1.5, and 2, respectively. The energy values are given with respect to $[N_{Si-Si}+(\hat{E}_{Si-O}/\hat{E}_{Si-Si})\times N_{Si-O}]$, where N_{Si-Si} and N_{Si-O} are the number of Si–Si and Si–O bonds and $\hat{E}_{Si-Si}$ and $\hat{E}_{Si-O}$ are strain energies per Si–Si (in *a*-Si) and Si–O (in *a*-SiO_2). For inset figures, the large (yellow) and small (red) balls represent Si and O atoms, respectively.

theory (DFT) program. The electron exchange-correlation energy was described within the generalized gradient approximation (GGA) [PW91 (Ref. 20)]. Vanderbilt-type ultrasoft pseudopotentials[21] were used for both Si and O atoms. A planewave cutoff energy of 300 eV was used. Brillouin zone sampling was performed using the Monkhorst-Pack scheme.[22] The convergence of calculation results with respect to cutoff energy and *k* point was carefully examined. Increasing the cutoff energy and the *k*-point mesh size to 400–450 eV and ($2\times2\times2$), respectively, resulted in no significant variation in the relative energies and atomic configurations of suboxide matrices considered. All atoms were fully relaxed using the conjugate gradient method until residual forces on constituent atoms become smaller than 0.02 eV/Å.

Figure 1 shows the variation in the relative energies of *a*-SiO_x (x=0–2) with respect to Si–Si and Si–O bond energies obtained from *c*-Si and *c*-SiO_2 (β-crystobalite), respectively. For each suboxide system, we considered two different atomic configurations, but their energy difference was minimal such that here we present the average values. The total increases in the relative energies of *a*-SiO_x can be decoupled in terms of the changes of suboxide energies and strain energies:

$$\Delta E_{total} = \Delta E_{subox} + \Delta E_{strain}.$$

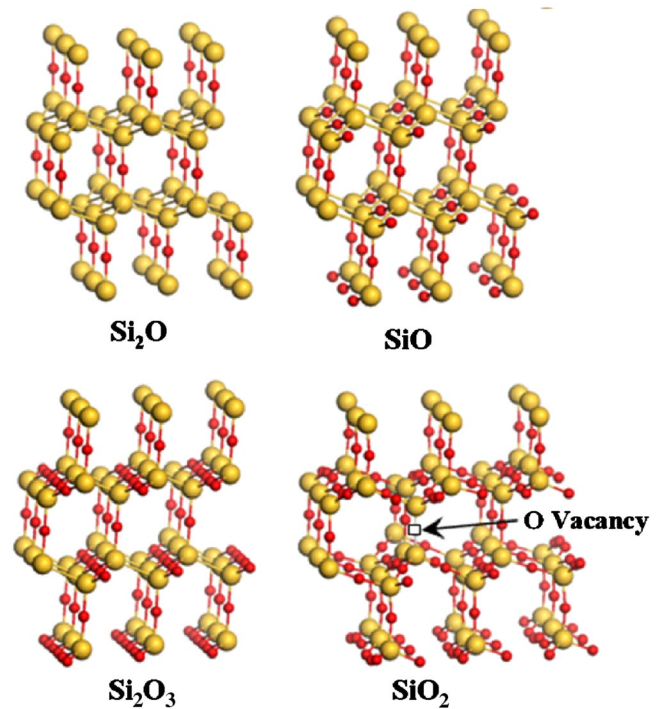

FIG. 2. (Color online) Schematic illustration of structural models for Si_2O, SiO, Si_2O_3, yielding Si atoms in +1, +2, +3 oxidation states, respectively, together with SiO_2 (with an oxygen vacancy as indicated). The large (yellow) and small (red) balls represent Si and O atoms, respectively.

The suboxide (penalty) energy (ΔE_{subox}), introduced by Hamann,[23] can represent the increase in Si–Si and Si–O bond energies due to incomplete O coordination. For a given suboxide system, the total suboxide energy can be evaluated by adding suboxide penalties associated with Si atoms in intermediate oxidation states (+1, +2, +3).[24] Using periodic Si^{1+}, Si^{2+}, and Si^{3+} model structures (as shown in Fig. 2), we obtained the penalty energies of 0.53 eV, 0.56 eV, and 0.28 eV for Si^{1+}, Si^{2+}, and Si^{3+}, respectively, in good agreement with previous DFT results.[23,24]

The strain energy (ΔE_{strain}) represents the increase in energy arising from lattice distortions, associated with bond stretching, bond angle bending, torsion strain, and nonbonding interactions (such as van der Waals interaction and electrostatic interaction). Here, for each suboxide system ΔE_{strain} is estimated by subtracting ΔE_{subox} from ΔE_{total}.

As expected the suboxide energy varies noticeably in a parabolic fashion with the Si:O ratio, but the variation in the strain energy turns out to be insignificant. This indicates that the phase separation in a suboxide matrix is mainly governed by suboxide penalty, with a minor contribution of strain. We, however, expect that strains induced at the nc-Si/SiO_x interface due to volume mismatch may influence the structural evolution of small Si clusters where the interface effect can be significant. The stability and crystallization of small Si clusters (<2 nm in diameter) are under investigation, but they are beyond the scope of this present paper.

III. ROLE OF SILICON AND OXYGEN DIFFUSION

We examined the role of Si and O diffusion in the phase separation of SiO_x. Suppose that O atoms undergo diffusion

Downloaded 02 Sep 2010 to 146.6.194.60. Redistribution subject to AIP license or copyright; see http://jap.aip.org/about/rights_and_permissions

TABLE I. O diffusion barriers (E_m in eV) used in KMC simulations for some selected events [$mnk \rightarrow (m-1)n(k+1)$, where m, n, and k are the initial oxidation states of Si_A, Si_B, and Si_C, respectively]. The values in bold are computed using crystalline Si^{1+}, Si^{2+}, Si^{3+} model structures (Ref. 23) as well as c-SiO_2 (O vacancy), as indicated. The rest are approximated by interpolating the computed values.

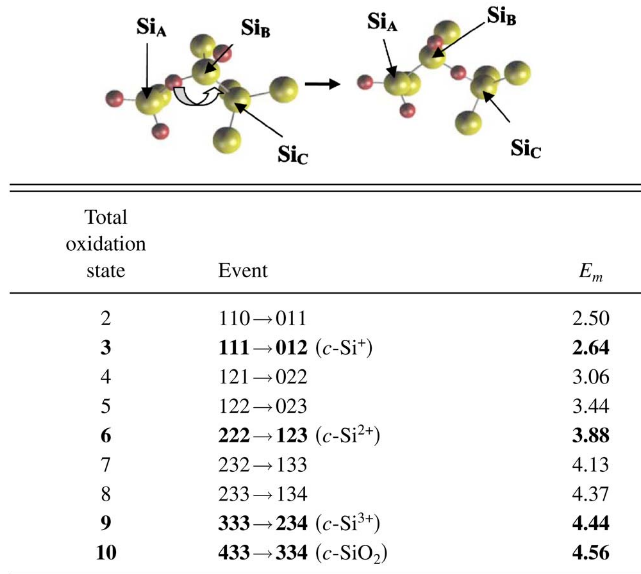

Total oxidation state	Event	E_m
2	$110 \rightarrow 011$	2.50
3	**$111 \rightarrow 012$** (c-Si^{+})	**2.64**
4	$121 \rightarrow 022$	3.06
5	$122 \rightarrow 023$	3.44
6	**$222 \rightarrow 123$** (c-Si^{2+})	**3.88**
7	$232 \rightarrow 133$	4.13
8	$233 \rightarrow 134$	4.37
9	**$333 \rightarrow 234$** (c-Si^{3+})	**4.44**
10	**$433 \rightarrow 334$** (c-SiO_2)	**4.56**

via hopping from a Si–Si bond center to another (which corresponds to O vacancy diffusion), the diffusion barrier is a function of the oxidation state of three Si lattice atoms (which are directly involved in the diffusion event, such as Si_A, Si_B, and Si_C in the schematic above Table I). As listed in Table I, the predicted barrier varies from 2.6 eV, 3.9 eV to 4.4 eV, respectively, in crystalline Si^{1+}, Si^{2+}, and Si^{3+} model systems (Fig. 2). The barrier for single O vacancy diffusion increases further to 4.6 eV in c-SiO_2. The O diffusion barriers were calculated using the nudged elastic band method (NEBM).[25] For each case, we initially sampled 16 intermediate images between two local minima along a diffusion path, and then determined the saddle point using the climbing NEBM method.[26] While varying from site to site in the amorphous matrix depending on the local geometry around the O vacancy site, the O hopping barrier is also primarily governed by the oxidation state of neighboring Si atoms. Our recent DFT studies[14] also showed that Si diffusion can be mediated by O vacancies which may convert to mobile SiO pairs and bond-centered Si atoms, and also create E'-type defects. Therefore, Si self-diffusion appears facilitated by O vacancies in a-SiO_2,[27] with an overall activation energy of 4.74 ± 0.25 eV.[28]

We should admit that diffusion of Si and O atoms in the Si-rich amorphous oxide matrix will be more complex than what we consider here, given existence of a high density of O vacancy related defects, such as E'-type defects particularly during high temperature annealing.[29] Irrespective of this, our previous DFT-GGA calculations[30] predicted that excess Si atoms prefer to exist in a-SiO_2 rather than c-Si (or at the c-Si/a-SiO_2 interface). This is consistent with earlier experiments[31] which demonstrated that most of Si atoms emitted from the c-Si/a-SiO_2 interface during thermal oxidation migrate into the a-SiO_2 part. Furthermore, the lifetime of diffusing intermediate states, such as bond-center Si or SiO pair, is very short because they easily transform into O vacancies with no sizable barrier. Thus, most of excess Si atoms likely remain as O vacancies in the a-SiO_2 matrix. This leads us to expect that the growth of Si nanopaticles will be controlled primarily by O outdiffusion from Si-rich regions rather than excess Si diffusion and agglomeration. However, it is also worth pointing out that Si diffusion will lead to a change in the spatial distribution of O vacancies, which may in turn affect indirectly the formation of Si nanoparticles.

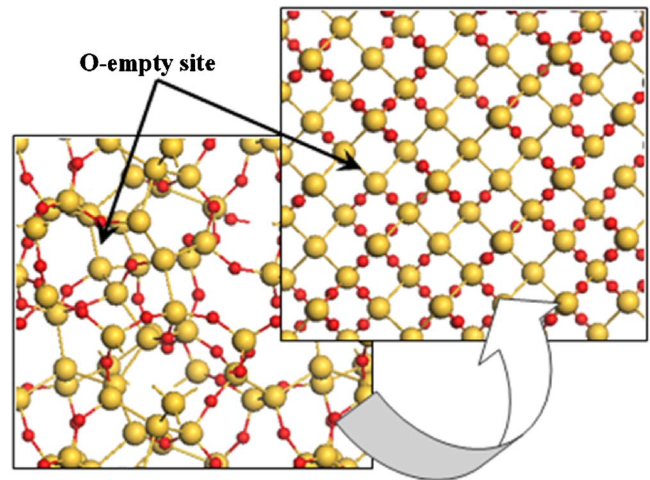

FIG. 3. (Color online) Schematic illustration of a Si suboxide model employed in KMC simulations. An amorphous suboxide matrix is simplified using a rigid diamond-lattice model, with Si atoms at the lattice sites and O atoms at the Si–Si bond centers. The large (yellow) and small (red) balls represent Si and O atoms, respectively.

IV. GROWTH MECHANISMS

Based on these fundamental findings, we developed a kinetic model for the formation of Si clusters in a Si suboxide matrix. Given that strain and Si diffusion play a minor role, as illustrated in Fig. 3, we can (1) simplify an amorphous suboxide structure using a rigid diamond-lattice model, with Si atoms at lattice sites and O atoms at Si–Si bond centers and (2) allow only O atoms to diffuse through O-empty sites. The oxidation state of each Si atom is evaluated by counting the number of its next neighboring O atoms. The magnitude of Si supersaturation is controlled by varying the number of O-empty sites.

For kinetic Monte Carlo (KMC) simulations, the barrier for O diffusion is given in terms of the oxidation states of three Si neighbors, (i.e., Si_A, Si_B, and Si_C as shown in the illustration above Table I). Si_A has four different oxidation states (from Si^{1+} to Si^{4+}), Si_B three oxidation states (from Si^{1+} to Si^{3+}), and Si_C four oxidation states (from Si^{0} to Si^{3+}). Hence, there are 48 ($=4 \times 3 \times 4$) combinations of oxidation state. Here, we approximate O diffusion barriers in the suboxide matrix by interpolating barriers computed for crystalline Si^{1+}, Si^{2+}, Si^{3+} model systems and crystalline Si (see Fig. 2). For a set of diffusion events having the same total oxidation state (of three Si neighbors), based on the case

Downloaded 02 Sep 2010 to 146.6.194.60. Redistribution subject to AIP license or copyright; see http://jap.aip.org/about/rights_and_permissions

with the highest suboxide energy, we approximate a barrier by interpolating the computed barriers, as listed in Table I. For a case having a lower suboxide energy, the corresponding diffusion barrier is estimated taking into account the energy gain with respect to the reference case (with the highest suboxide energy in each set of the same total oxidation state). For instance, O diffusion from the oxidation state of $(S_A, S_B, S_C = +1, +1, +1)$ to $(0, +1, +2)$ is assumed to require overcoming a barrier of 2.64 eV, with a return barrier of 3.14 eV ($= 2.64 - \Delta E_{\mathrm{subox}}$, where the suboxide energy difference between the initial and the final states is $\Delta E_{\mathrm{subox}} = -0.5$ eV). Note that for the total oxidation state of +3 the combination of $(+1, +1, +1)$ yields the highest suboxide penalty energy.

In addition, a penalty energy of 0.5 eV is considered when an O atom diffuses into a crystallized Si region. This is to take into account the relative energy of O atom in between amorphous and crystalline Si layers; that is, our DFT-GGA calculation predicts that O atoms prefer to exist in *a*-Si, rather than in *c*-Si, with an energy gain of 0.5 eV/atom. While no definitive kinetic model for crystallization of embedded Si clusters is available, here we assume that Si clusters larger than 2 nm (in diameter) are crystallized within a few seconds of annealing.

With the approximated barriers, O diffusion rates are evaluated by $D = D_0 \exp(-E_m / k_B T)$, where D_0 is the prefactor, E_m is the diffusion barrier, k_B is the Boltzmann constant, and T is the substrate temperature. Here, the prefactor D_0 is assumed to be 2.6 cm^2/s.[32] At each KMC step, one diffusion event is chosen to take place according to its probability, and the KMC simulation time (t_{KMC}) is advanced by

$$\Delta t_{\mathrm{KMC}} = -\ln Z / \Sigma R_i,$$

where Z is a random number ranging from 0 to 1, and R_i $[= \nu_0 \exp(-E_m / kT)]$ is the rate constant for the *i*th event. The effective O jumping frequency is given as $\nu_0 = (6D_0/\lambda^2)^{1/2}$, where the jumping distance λ is set to be 2.6 Å.

This simplified diffusion model, yet physically sound, should be sufficient for identifying mechanisms underlying the formation of Si clusters in a suboxide matrix. However, we should also admit the limitation of current model in describing the structural evolution of embedded Si clusters with annealing time, which requires further investigations into Si cluster crystallization and O diffusion at various oxidation and defect conditions.

Using the simple kinetic model, we performed KMC simulations for three different levels of Si supersaturation, 10%, 20%, and 30%. Figure 4 shows a series of snapshots from the simulations. Here, while the number of Si atoms (at the lattices) is kept constant at 27 000, the number of O atoms (at the bond centers) varies according to the Si:O ratio. Initially, O atoms are randomly distributed. For the same KMC annealing time (t_{KMC}) at 1373 K, the diameter of Si clusters increases substantially with the degree of supersaturation, consistent with experiments.[12] Fernandez *et al.*[12] also attempted to explain the strong correlation between the cluster size and the initial superstauration by introducing cluster-cluster interactions into the Ostwald ripening model (based on excess Si diffusion and agglomeration). While the proximity effect is still uncertain, our growth model (based on O outdiffusion) explains well the correlation between the Si cluster size and initial supersaturation.

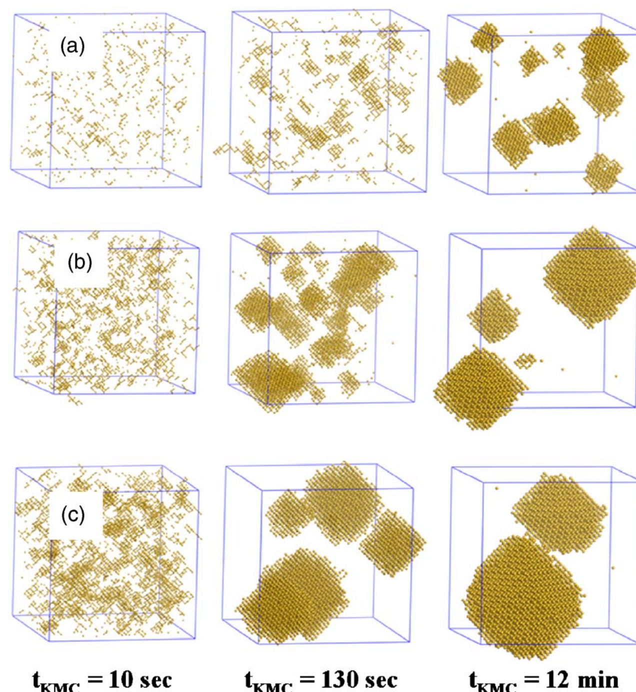

FIG. 4. (Color online) Series of snapshots from KMC simulations of phase separation in Si suboxide with the initial Si supersaturation of (a) 10%, (b) 20%, and (c) 30% at 1100 °C. Here, only Si^0 atoms are displayed. The box size is $8.1 \times 8.1 \times 8.1$ nm^3.

From KMC simulations, we have also found that at the initial stage of annealing a number of small Si clusters start to form via O outdiffusion. A high density of small clusters leads them to join together to grow, through continued O outdiffusion from Si-rich regions. Most of the small clusters are somewhat elongated rather than spherical. As the cluster size gets larger while the cluster density is lower, Si clusters become gradually more compact. Our KMC simulations clearly demonstrate that the formation of Si clusters occurs rapidly by O outdiffusion from Si-rich regions at the early stage of annealing.

When two clusters exist closely with a sufficient amount of O vacancies between them, they can be connected via O outdiffusion from the gap region, as shown in Fig. 5. The combined cluster rearranges itself to form a compact shape through O diffusion along the cluster-matrix interface, lowering the suboxide energy by reducing the interface area. Note that the interface commonly has a higher suboxide energy. This may look like a conventional coalescence process; however, the clusters do not move toward each other as mentioned above. Hereafter, this growth process is referred to as "coalescencelike," as opposed to conventional coalescence. The coalescencelike behavior is mainly responsible for Si cluster growth at the early stage of annealing where the cluster density is sufficiently high.

As demonstrated in Fig. 6, from KMC simulations we have also identified that larger Si clusters grow at the expense of smaller ones. This phenomenon resembles "Ostwald ripening;" however, it turns out that smaller clusters shrink

Downloaded 02 Sep 2010 to 146.6.194.60. Redistribution subject to AIP license or copyright; see http://jap.aip.org/about/rights_and_permissions

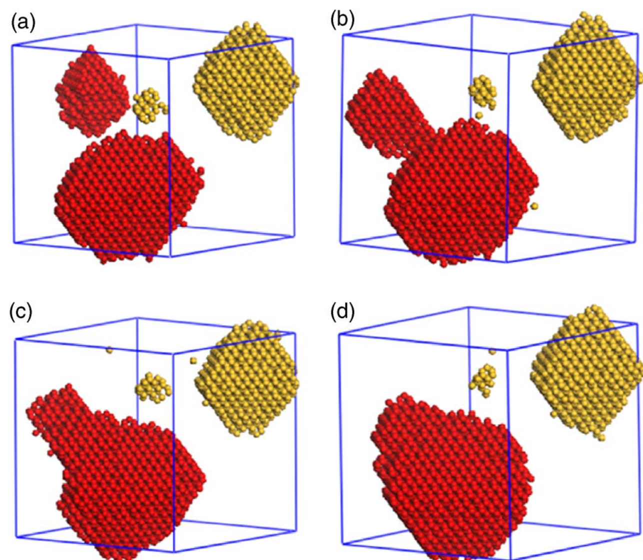

FIG. 5. (Color online) Illustration of "coalescencelike" growth (in red) occurring in a KMC simulation of phase separation in Si suboxide with 30% initial Si supersaturation at 1100 °C. (a) $\Delta t_{KMC}=0.0$ s; (b) $\Delta t_{KMC}=4.0$ s; (c) $\Delta t_{KMC}=8.3$ s; (d) $\Delta t_{KMC}=14.3$ s. Here, only Si^0 atoms are displayed. The box size is $8.1\times 8.1\times 8.1$ nm^3.

and eventually disappear by reoxidation, not by dissolution. That is, as phase separation proceeds, an increase in the matrix oxidation state leads to reoxidation of smaller Si clusters during high temperature annealing. We refer to this growth behavior as "pseudo-Ostwald ripening," as opposed to conventional Ostwald ripening. This pseudoripening process becomes important when the density of clusters is low so that they are separated by large distances. Our KMC simulations predict that the ripening process takes place several orders of magnitude slower than the coalescencelike growth. This is

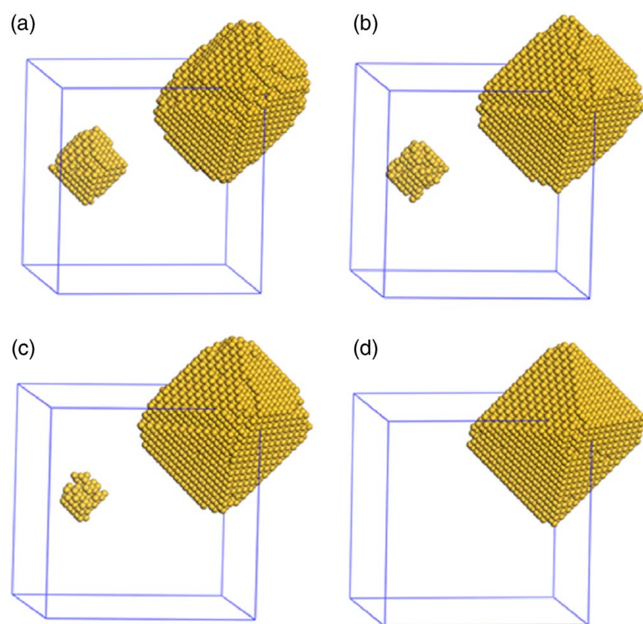

FIG. 6. (Color online) Illustration of "pseudo-Ostwald ripening" occurring in a KMC simulation of phase separation in Si suboxide with 20% initial Si supersaturation at 1100 °C. (a) $\Delta t_{KMC}=0.0$ h; (b) $\Delta t_{KMC}=23.1$ h; (c) $\Delta t_{KMC}=23.3$ h; (d) $\Delta t_{KMC}=23.4$ h. Here, only Si^0 atoms are displayed. The box size is $8.1\times 8.1\times 8.1$ nm^3.

not surprising considering the difficulty of nc-Si reoxidation. The KMC result is consistent with experiments that show the fast growth of Si clusters at the early state of annealing, followed by slow ripening.[12] Our study also suggests that the coalescencelike behavior is mainly responsible for the big variation of Si cluster size with the Si:O ratio.

V. SUMMARY

We present the underlying mechanism of Si nanocrystal formation in an amorphous Si suboxide matrix based on extensive first-principles-based atomistic modeling. The theoretical effort includes density functional calculations for determining the energetics of suboxide matrices with varying Si:O ratios and the structure and diffusion of single O and Si atoms in the suboxide system, metropolis Monte Carlo simulations for generating the structure of amorphous Si suboxides, and kinetic Monte Carlo simulations for identifying the formation mechanism of Si nanoclusters in a Si suboxide matrix. The results predict that the formation of oxide embedded Si clusters is primarily attributed to chemical phase separation to Si and SiO_2, which is mainly driven by suboxide penalty, with a minor contribution of strain. The phase separation turns out to be primarily controlled by diffusion of O atoms rather than Si atoms. From kinetic Monte Carlo simulations based on these fundamental findings, we have identified two growth mechanisms: "coalescencelike" and "pseudo-Ostwald ripening." The former is mainly responsible for fast Si cluster growth at the early stage of annealing where the clusters are close to each other, while the latter becomes important when the density of clusters is low such that they are separated by large distances. Our simulation results also show that the ripening process takes place several orders of magnitude slower than the coalescencelike growth, and the prevailing coalescencelike growth behavior results in a big variation in the Si cluster size with the Si:O ratio. The results agree well with experimental observations that show strong dependence of the cluster size on the initial Si supersaturation as well as rapid formation of Si clusters at the early stage of annealing with very slow ripening. While the simple but physically sound growth model presented here explains well the intriguing growth behavior of Si nanoclusters in amorphous Si suboxide, further investigations into Si cluster crystallization and O diffusion rates at various oxidation/defect conditions are required to develop an improved kinetic model for precise description of the structural evolution of embedded Si nanoclusters.

ACKNOWLEDGMENTS

The authors greatly acknowledge the National Science Foundation (CAREER-CTS-0449373 and ECS-0304026) and the Welch Foundation (F-1535) for their financial support. They would also like to acknowledge the Texas Advanced Computing Center for use of their computing resources.

[1]W. L. Wilson, P. F. Szajowski, and L. E. Brus, Science **262**, 1242 (1993).
[2]Y. Kanemitsu, T. Ogawa, K. Shiraishi, and K. Takeda, Phys. Rev. B **48**, 4883 (1993).
[3]S. Tiwari, F. Rana, K. Chan, L. Shi, and H. Hanafi, Appl. Phys. Lett. **69**,

Downloaded 02 Sep 2010 to 146.6.194.60. Redistribution subject to AIP license or copyright; see http://jap.aip.org/about/rights_and_permissions

1232 (1996).
[4]R. J. Walters, P. G. Kik, J. D. Casperson, H. A. Atwater, R. Lindstedt, M. Giorgi, and G. Bourianoff, Appl. Phys. Lett. **85**, 2622 (2004).
[5]L. Pavesi, L. Dal Negro, C. Mazzoleni, G. Franzo, and F. Priolo, Nature (London) **408**, 440 (2000).
[6]H. S. Rong, R. Jones, A. S. Liu, O. Cohen, D. Hak, A. Fang, and M. Paniccia, Nature (London) **433**, 725 (2005).
[7]P. Pellegrino, B. Garrido, C. Garcia, J. Arbiol, J. R. Morante, M. Melchiorri, N. Daldosso, L. Pavesi, E. Scheid, and G. Sarrabayrouse, J. Appl. Phys. **97**, 074312 (2005).
[8]L. C. Kimerling, L. Dal Negro, S. Saini, Y. Yi, D. Ahn, S. Akiyama, D. Cannon, J. Liu, J. G. Sandland, D. Sparacin, J. Michel, K. Wada, and M. R. Watts, *Silicon Photonics* (Springer-Verlag, Berlin, 2004).
[9]G. Ghislotti, B. Nielsen, P. AsokaKumar, K. G. Lynn, A. Gambhir, L. F. DiMauro, and C. E. Bottani, J. Appl. Phys. **79**, 8660 (1996).
[10]W. Skorupa, R. A. Yankov, I. E. Tyschenko, H. Frob, T. Bohme, and K. Leo, Appl. Phys. Lett. **68**, 2410 (1996).
[11]T. Shimizu-Iwayama, N. Kurumado, D. E. Hole, and P. D. Townsend, J. Appl. Phys. **83**, 6018 (1998).
[12]B. G. Fernandez, M. Lopez, C. Garcia, A. Perez-Rodriguez, J. R. Morante, C. Bonafos, M. Carrada, and A. Claverie, J. Appl. Phys. **91**, 798 (2002).
[13]T. Muller, K. H. Heinig, and W. Moller, Appl. Phys. Lett. **81**, 3049 (2002).
[14]D. Yu, G. S. Hwang, T. A. Kirichenko, and S. K. Banerjee, Phys. Rev. B **72**, 205204 (2005).
[15]F. Wooten, K. Winer, and D. Weaire, Phys. Rev. Lett. **54**, 1392 (1985).
[16]K. Laaziri, S. Kycia, S. Roorda, M. Chicoine, J. Robertson, J. Wang, and S. Moss, Phys. Rev. B **60**, 13520 (1999).
[17]A. Brunet-Bruneau, D. Souche, S. Fisson, V. N. Van, G. Vuye, F. Abeles, and J. Rivory, J. Vac. Sci. Technol. A **16**, 2281 (1998).
[18]Y. Tu and J. Tersoff, Phys. Rev. Lett. **84**, 4393 (2000).
[19]G. Kresse and J. Furthmuller, *Vasp the Guide* (Vienna University of Technology, Vienna, Austria, 2001).
[20]J. P. Perdew and Y. Wang, Phys. Rev. B **45**, 13244 (1992).
[21]D. Vanderbilt, Phys. Rev. B **41**, 7892 (1990).
[22]H. J. Monkhorst and J. D. Pack, Phys. Rev. B **13**, 5188 (1976).
[23]D. Hamann, Phys. Rev. B **61**, 9899 (2000).
[24]A. Bongiorno and A. Pasquarello, Phys. Rev. B **62**, R16326 (2000).
[25]G. Mills and H. Jonsson, Phys. Rev. Lett. **72**, 1124 (1994).
[26]G. Henkelman, B. P. Uberuaga, and H. Jonsson, J. Chem. Phys. **113**, 9901 (2000).
[27]M. Uematsu, H. Kageshima, Y. Takahashi, S. Fukatsu, K. M. Itoh, K. Shiraishi, and U. Gosele, Appl. Phys. Lett. **84**, 876 (2004).
[28]D. Tsoukalas, C. Tsamis, and P. Normand, J. Appl. Phys. **89**, 7809 (2001).
[29]*Structure and Imperfections in Amorphous and Crystalline Silicon Dioxides*, edited by R. A. B. Devine, J.-P. Duraud, and E. Dooryhee (Wiley, New York, 2000).
[30]T. A. Kirichenko, D. Yu, S. K. Banerjee, and G. S. Hwang, Phys. Rev. B **72**, 035345 (2005).
[31]K. Taniguchi, Y. Shibata, and C. Hamaguchi, J. Appl. Phys. **65**, 2723 (1989).
[32]J. C. Mikkelsen, Appl. Phys. Lett. **45**, 1187 (1984).

Downloaded 02 Sep 2010 to 146.6.194.60. Redistribution subject to AIP license or copyright; see http://jap.aip.org/about/rights_and_permissions